Solution 1 H NMR Characterization of the Axial Bonding of the Two His in Oxidized Human Cytoglobin

ARTICLE *in* JOURNAL OF THE AMERICAN CHEMICAL SOCIETY · NOVEMBER 2006

Impact Factor: 12.11 · DOI: 10.1021/ja063330d · Source: PubMed

Published in final edited form as:
J Am Chem Soc. 2006 October 4; 128(39): 12988–12999. doi:10.1021/ja063330d.

Solution ^{1}H NMR characterization of the axial bonding of the two His in oxidized human cytoglobin

Vasyl Bondarenko[†], **Sylvia Dewilde**[§], **Luc Moens**[§], and **Gerd N. La Mar**[†,*]

† *Department of Chemistry, University of California, Davis, CA 95616*

§ *Department of Biomedical Sciences, University of Belgium, Universiteitsplein 1, B-2610 Wilrijk (Anterwerpen) Belgium*

Abstract

Solution ^{1}H NMR spectroscopy has been used to determine the relative strengths (covalency) of the two axial His-Fe bonds in paramagnetic, S = 1/2, human met-cytoglobin. The sequence specific assignments of crucial portions of the proximal and distal helices, together with the magnitude of hyperfine shifts and paramagnetic relaxation, establish that His81 and His113, at the canonical positions E7 and F8 in the myoglobin fold, respectively, are ligated to the iron. The characterized complex (~90%) in solution has protohemin oriented as in crystals, with the remaining ~10% exhibiting the hemin orientation rotated 180° about the α-, γ-meso axis. No evidence could be obtained for any five-coordinate complex (<1%) in equilibrium with the six-coordinate complexes. Extensive sequence-specific assignments on other dipolar shifted helical fragments and loops, together with available alternate crystal coordinates for the complex, allowed the robust determination of the orientation and anisotropies of the paramagnetic susceptibility tensor. The tilt of the major axis is controlled by the His-Fe-His vector, and the rhombic axes by the mean of the imidazole orientations for the two His. The anisotropy of the paramagnetic susceptibility tensor allowed the quantitative factoring of the hyperfine shifts for the two axial His to reveal indistinguishable pattern and magnitudes of the contact shifts or π spin densities, and hence, indistinguishable Fe-imidazole covalency for both Fe-His bonds.

Keywords

cytoglobin; axial bond strength; contact shift; magnetic axes; magnetic anisotropy; hyperfine shifts

INTRODUCTION

Vertebrate globins, in particular hemoglobin, Hb,[1] and myoglobin, Mb, are O_2 carriers and O_2 storage proteins found in diverse species. [2–4] They represent one of the most extensively studied class of folded proteins. In the more common form, globins appear as ~150 residue proteins consisting of 8 helices (A-H) in a characteristic fold where the heme binds to the protein through a single protein ligand, the proximal His(F8) (eighth position on helix F), with the distal side available for exogenous ligation by small molecules. This conserved fold is found in both monomeric and oligomeric globins. Shorter (truncated) globins of ~100 residue also have been characterized which retain less than the eight helices, and exhibit a specific portion of the "Mb fold". [5–9] More recently, a new class of globins has been identified consisting of both normal length [10–14] and truncated Hbs [15–17] for which the protein provides two His ligands to the heme to render a coordinately saturated chromophore in the absence of

e-mail: lamar@chem.ucdavis.edu.

exogenous ligand for both the reduced and oxidized forms. These six-coordinate globins are found in non-symbiotic plants, [10] cyanobacteria, [16–18] insects [13] and most surprisingly, in mammals, [11–15, 19] and a combination of mutagenesis and structural characterization has shown that the sixth endogenous ligand is His(E7). The existence of a six-coordinate "deoxy" globin introduces yet another mechanism of control of function in that the ligation on-rate must be preceded by the rupture of the His(E7)-iron bond. [10, 20, 21]

Neuroglobin, [22] Ngb, and cytoglobin, [23–25] Cygb, are two new members of the vertebrate globin family which exhibit only limited sequence homology to Mb or Hb and for which a distal His is capable of forming a sixth bond to the heme iron in both the functional, reduced or oxidized oxidation states. [26, 27] Ngb is a ~150 residue protein expressed primarily in the brain and retina of the eye. [26] Cygb expressed in diverse tissues with unknown function, [23, 24, 26, 27] is a ~190 residue globin for which the central ~150 residues exhibit sequence homology to Mb and Hb. Both exhibit O_2 affinity that is similar to that of Mb. The factors that control the distal His E7 bond scission are incompletely understood and constitute an active area of globin research. [20–22, 28] One obvious possibility is that the distal His-Fe bond is intrinsically strained in the deoxy state. Both Ngb and Cygb have been shown [29] to form disulfide bonds between two Cys, and in the case of Ngb, the O_2 affinity, and hence the His-Fe bond scission rate changes [27, 29] by a factor of 10 (only a factor ~2 in Cygb). Two crystal structures of metCygb have been reported, one for the human double-mutant C38S/C83S-metCygb that abolishes the potential disulfide link [11, 29] and another of human wild-type metCygb. [12] The dominant six-coordinate form in the former, [11] and the sole six-coordinate form in the latter [12] have the distal Fe-His(E7) bond slightly longer (but within experimental uncertainty) than the Fe-His(F8) bond. Some evidence for an intrinsically weak Fe-His(E7) bond could be inferred from the observation that, for one of the two inequivalent molecules in the unit cell, the populations of six-coordinate and five-coordinate, with the Fe-His(E7) bond ruptured, [11] are 55% and 45%, respectively.

Spectroscopy can aid in the detailed characterization of axial ligand bonds in hemoproteins, either by detection of the strength of the bond as revealed in the characteristic Fe-His bond vibration in resonance Raman spectra, [30–32] or the Fe-His covalency as observed in a paramagnetic derivative via ^{1}H NMR spectroscopy. [33, 34] The latter technique is particularly well-suited to such a study, since the contact shift, δ_{con}, that results for π spin transfer from the His imidazole ring to the iron directly monitors the bond covalency. [34, 35] Analyses of the contact contributions to the hyperfine shifts of ligated His in both cyanomet globins [34] and ferricytochrome [36] have revealed that the unpaired p spin resides in the highest filled p MO of the imidazole ring, which results in the largest detectable π spin density at C_ε (resulting in an upfield $C_\varepsilon H$ contact shift), somewhat less π spin density in C_γ (resulting in upfield $C_\beta H$ contact shift). The low-spin, ferric or metCygb complex is well-suited for such a NMR study, since the paramagnetism results in significant chemical shift dispersion in the active site due to hyperfine shifts, δ_{hf}, that will resolve the two axial His resonance. [34] At the same time, this oxidation/spin state introduces only weak to moderate paramagnetic relaxation that does not seriously interfere with the definitive characterization of solution molecular and electronic studies by appropriately tailored 1D/2D NMR. [34, 37, 38] The large anisotropy of low-spin iron(III) heme also results in substantial dipolar shifts, δ_{dip}, for both the ligated and non-ligated active site residues. Thus δ_{dip} is the only source of δ_{hf} for non-ligated residues, but for the heme and axial ligand, δ_{dip} contributes significantly to δ_{hf} according to:

$$\delta_{hf}=\delta_{con}+\delta_{dip} \quad (1)$$

In order to determine δ_{con} for the two His, which is directly proportional to Fe-His covalency, it is first necessary to quantitatively determine δ_{dip}, which is given by:[34, 39, 40]

$$\delta_{dip}=(24\pi\mu_o N_A)^{-1}\{3\Delta\chi_{ax}(\cos^2\theta' - 1)R^{-3}+2\Delta\chi_{rh}\sin^2\theta'\cos2\Omega' R^{-3}\}\Gamma(\alpha,\beta,\gamma) \quad (2)$$

where R, θ′, Ω′ (x′, y′, z′) are the coordinates of a given proton in an iron-centered, reference coordinate system (as provided by crystallography), $\Delta\chi_{ax}$ and $\Delta\chi_{rh}$ are the axial and rhombic anisotropies of the paramagnetic susceptibility tensor, χ, in the magnetic coordinate system, x, y, z, where χ is diagonal, and Γ(α, β, γ) is the Euler rotation that converts the reference coordinate system, x′, y′, z′, into the magnetic axes, x, y, z. The three Euler angles α, β and κ ~ α + γ represent the direction of the tilt of the major magnetic axes from the heme normal, the magnitude of this tilt, and the location of the rhombic axes, as shown in Figure 1.

Our interests in this report are to characterize in detail by ^{1}H NMR the active site molecular and electronic structure of metCygb in solution, explore the utility of hyperfine shifts for the axial His to quantitatively compare the Fe-His bonds for the proximal and distal His, and assess the presence in solution of equilibrium, five-coordinate derivatives with the Fe-His(E7) bond ruptured, such as observed for a minor population of molecules in the C385/C835-met-Cygb crystal structure,[11] and as expected as an intermediate in the process of exogenous ligand binding.

EXPERIMENTAL METHODS

Sample preparation

The metCygb sample was prepared as described in detail previously. [29] Two WT human metCygb samples (the first one in 90% ^1H_2O and 10% ^2H_2O and the second one in 90% ^2H_2O and 10% ^1H_2O), pH7.5 in 50mM phosphate buffer were prepared for the ^{1}H NMR study. The concentration of the sample in ^1H_2O was ~2.5 mM and that one in ^2H_2O ~0.2 mM.

NMR spectroscopy

^{1}H NMR spectra were collected in ^1H_2O and ^2H_2O on either Bruker Avance 500 or 600 spectrometers operating at 500 or 600 MHz, respectively. Reference spectra were collected over the temperature range 5 – 35°C at repetition rates of 1 – 5 s^{-1} over 10 – 100 kHz spectral windows using a standard one-pulse sequence with saturation of the water solvent signal. The chemical shifts were referenced to 2,2′-dimethyl-2-silapentane-5-sulfonate (DSS) through the water peak calibrated at each temperature. The spectra were exponentially apodized with 5 Hz line broadening. Non-selective T_1 values for the resolved peaks were determined from the null in the standard inversion-recovery experiment ($T_1 \sim \tau_{null}/\ln 2$) at repetition rate of 1 s^{-1}. The rapidly relaxing signals were selectively enhanced in WEFT spectra [41] at a repetition rate of 10 or 5 s^{-1} with a relaxation delay of 1 - 100 ms, where the slowly relaxing diamagnetic envelope was suppressed. Steady state NOE spectra upon saturating the heme methyl peaks were collected in ^1H_2O at 600 MHz with a repetition rate of 1.5 s^{-1} and a 300 ms irradiation time. The spectra were exponentially apodized with 10 Hz line broadening. WEFT-NOE spectra [37] upon saturating the rapidly relaxing signal His81(E7) $N_\varepsilon H$ were collected at 500 MHz in ^1H_2O with a repetition rate of 10 s^{-1}, a 45 ms relaxation delay and a 50 ms irradiation time. The spectra were exponentially apodized with 20 Hz line broadening.

NOESY spectra [42] were collected in ^1H_2O at 600 MHz at 18, 25, 30 and 35°C with a repetition rate of 1 s^{-1} and mixing time τ_m = 60 ms, using 512 t_1 blocks and 2048 t_2 points. Spectral windows were 19 kHz at 25 and 35°C and 11 kHz at 18 and 30°C. CLEAN-TOCSY spectra [43] were recorded in ^1H_2O on the 500 MHz spectrometer at 25°C with a 6 kHz bandwidth, a 40 ms mixing time, and a repetition rate of ~1.2 s^{-1}, at 30°C with a 8 kHz bandwidth, a 22 ms mixing time, and a repetition rate 0.8 s^{-1}, and at 35°C with a 6 kHz bandwidth, a 40 ms mixing time, with a repetition rate 0.8 s^{-1}, as well with a 10 kHz bandwidth, a 25 ms mixing time, and a repetition rate of 1 s^{-1}, all using 512 t_1 blocks and 2048 t_2 points. The 2D data set were

processed using Bruker XWIN software on a Silicon Graphics Indigo work station and consisted of 30°-shifted-sine-squared-bell apodization in both dimensions, and zero-filling to 2048x2048 data points prior to Fourier transformation.

Magnetic axes determination

The location of the magnetic axes was determined by finding the Euler rotation angles, Γ(α, β, γ), that convert the crystal–structure based, iron-centered reference coordinate system, x′, y′, z′, into the magnetic coordinate system, x, y, z, where the paramagnetic susceptibility tensor, χ, is diagonal, and α, β, γ, are the three Euler angles. [34, 39, 44] The angle β dictates the tilt of the major axis, *z*, from the heme normal z′, α reflects the direction of this tilt, and is defined as the angle between the projection of the *z* axis on the heme x′, y′ plane and the x′ axis (Figure 1A), and $\kappa \approx \alpha+\gamma$ is the angle between the projection of the x axis onto the heme x′, y′ plane and the x′ axis, and locates the rhombic axes (Figure 1A). Magnetic axes were determined by a least-square search for the minimum in the error function, F/N:

$$F/n=\sum[(\delta_{dip}(obs)-\delta_{dip}(calc))]^2 \quad (3)$$

where the calculated dipolar shift, δ_{dip}(calc), in the reference coordinate system, x′, y′, z′, (or R, θ′, Ω′) is given by Eq. (2). The observed dipolar shift, δ_{dip}(obs), is given by:

$$\delta_{dip}(obs)=\delta_{DSS}(obs)-\delta_{DSS}(dia) \quad (4)$$

where δ_{DSS}(obs) and δ_{DSS}(dia) are the chemical shifts, in ppm, referenced to DSS, for the paramagnetic metCygb complex, and an isostructural diamagnetic complex, respectively. Since the experimental data on the latter one are not available, reasonable chemical shift can be determined with values using the ShiftX program [45] and adding the ring current chemical shift induced by the heme [46] using the alternate crystal structure. [11, 12] For the ring protons of aromatic residues not covered in the Shift X program, [45] the δ_{DSS}(dia) was calculated as described in detail previously. [40] The contact shift for the heme and the axial histidine protons can be obtained by:

$$\delta_{con}=\delta_{DSS}(obs)-\delta_{DSS}(dia)-\delta_{dip}(calc) \quad (5)$$

RESULTS

The resolved portions of the 600 MHz ^{1}H NMR spectrum of metCygb in ^1H_2O are shown in Figure 2A. The spectrum consists of six (three upfield, three low-field) resolved methyl peaks and numerous resolved, single-proton peaks that argue for a single, dominant (>90%) molecular species. There are detected several other weak peaks from a clearly minor component, whose intensities represent the likely methyls for a $\lesssim$ 10% minor component. Several of the resolved, low-field, single proton peaks are strongly relaxed, as is obvious in the WEFT trace in Figure 2B. Three very broad and strongly relaxed linewidths ~500 Hz, (T_1 ~ 3 ms) are observed, of which the two upfield peaks at −5 ppm (marked Y in Figure 2B) and at −9.5 ppm (labeled H81ε) exhibit intensities consistent with arising from one proton each, while the partially resolved low-field peak at ~16 ppm (marked X in Figure 2B) has intensity indicative of more than one proton. Such broad and strongly relaxed protons must arise from the four non-labile ring protons of the two ligated His. [44] Several low-field resonances exhibit $T_1 \leq 50$ ms, of which that at 18.1 ppm (T_1 ~20 ms), among others in the window 9–20 ppm, is lost in the spectrum in ^2H_2O (Figure 2C). The T_1 for resolved signals are listed in Tables 1 and 2.

Assignment of the heme

TOCSY spectra (not shown; see Supporting Information) locate one CH-CH_2, one CH_2-CH_2, and one vinyl group with significant temperature dependence to the shifts to indicate

origins as heme substituents. The fourth proton to the CH-CH_2 fragment (as well as the protons of the other vinyl group) are outside the spin-lock field of the TOCSY spectrum, but an intense NOESY cross peak indicative of geminal protons (Figure 3D), and characteristic low-field resolved $C_\alpha H$ to an upfield resolved $C_\beta H_2$ of a vinyl (Figure 3A), identify the four non-methyl heme substituents. Two of the three low-field resolved methyls exhibit the weak inter-methyl NOESY cross peak of 1-CH_3 and 8-CH_3 (Figure 3E), and NOESY contact of the former with a vinyl (Figure 3A) and the latter with a CH_2-CH_2 (Figure 3C) fragment identify the 2-vinyl (and hence 4-vinyl) and 7-propionate (and hence 6-propionate) heme signals. NOESY cross peaks of a CH_2-CH_2 fragment to the remaining resolved methyl peaks at 36 ppm (not shown) identify 5-CH_3. The remaining TOCSY-detected 4-vinyl group exhibits NOESY cross peaks to a non-resolved methyl group with no scalar connectivity (not shown), and with characteristic anti-Curie behavior (see Supporting Information) to provide the remaining 3-CH_3 resonance position. NOESY cross peaks from the substituents adjacent to a meso position to relaxed peaks, with characteristic strongly low-field intercepts (~15–20 ppm) in a Curie plot, locate the four meso-Hs. The chemical shifts for the heme resonances are listed in Table 1.

Sequence-specific assignment of the proximal and distal helices

We use the helical/loop position of residues in the standard Mb fold as described by sperm whale Mb [2,3] since this provides direct comparison of the pattern of dipolar shifts for the similarly placed residue relative to the heme.

At least the peptide NH and one $C_\beta H$ of a ligated His can be expected to yield resonances resolved to the low-field of 10 ppm. [34] Two such $C_\beta H$ protons are resolved in the low-field trace, and their T_1 ~50 ms, dictate that they are significantly closer to the iron than a heme methyl (T_1 ~100 ms), and hence originate from coordinated His. TOCSY spectra reveal protons of two such low-field $NHC_\alpha H$-$C_\beta H$ fragments, as illustrated in Figure 4 (the $C_\alpha H$ and $C_\beta H$ of one His are essentially degenerate). The second $C_\beta H$ is not detected in TOCSY spectra because of insufficient power in the spin lock field, but is very readily detected in the NOESY spectrum by the intense cross peak indicative of geminal protons (Figure 3D). The TOCSY/NOESY connectivities and chemical shifts are very similar to those observed for the two His in metNgb.[48]

Six helical fragments are detected by their characteristic [49] N_i-N_{i+1}, α_i-N_{i+1}, β_i-N_{i+1}, α_i-N_{i+3} and/or α_i-β_{i+3} NOESY cross peaks among TOCSY detected spin systems. The N_i-N_{i+1} and α_i-N_{i+1} connections for the fragments of the proximal and distal helices are illustrated in Figure 5. One fragment is represented by Val_i-Gly_{i+1}-Z_{i+2}-Ala_{i+3}-AMX_{i+4}-Ala_{i+5}-Leu_{i+6} (z is >4 spins) (connections are summarized in Figure 6), with one of the His backbone presented above as AMX_{i+4}. The sequence identifies this uniquely as Val109-Leu115 and residues F4-F10 of the proximal or F helix. Hence the hyperfine shifted backbone of His113(F8) is assigned. The side chains exhibits all expected NOESY cross peaks to the heme, as shown schematically in Figure 1B. In addition to His113(F8), significant hyperfine shifts are observed for Val109(F4), Gly110(F5), Ala112(F7), and Ala114(F9) (see Table 2). The NOESY spectrum exhibits a cross peak of the His113(F8) $C_\beta H$s and NH to a moderately relaxed (T_1 ~20 ms), labile proton at 18.4 ppm (Figure 3F) which identifies the His ring $N_\delta H$. Chemical shifts for the axial His are listed in Table 1, those for the strongly dipolar shifted residues are listed in Table 2, with the remaining data provided in Supporting Information (Table S1).

The helical fragment which contains the other axial His AMX spin system (as residue j+3) exhibits the sequential NOESY cross peaks (Figure 5) represented by: $(Leu)_j$-$(N\alpha)_{j+1}$-$(N\alpha)_{j+2}$-$(AMX)_{j+3}$-Ala_{j+4}-$(N\alpha)_{j+5}$-Z_{j+6}-$(Val/Thr)_{j+7}$, which the sequence identifies as the distal helical fragment Leu78-Val85 as residues E4-E14 on the distal or E helix. An additional fragment represented by Ala_k-Leu_{k+1}-$(N\alpha)_{k+2}$-Val_{k+3} must arise from the nearby distal helix fragment Ala88(E14)-Asn88(E16). The residues exhibit the expected[11, 12] NOESY contacts

to the heme as depicted in Figure 1B. It was not possible to locate any other resolved and relaxed protons with NOESY connections to the His81(E7) backbone as would be expected for its ring $N_\delta H$, and as is observed for His113(F8) in Figure 3F, or for the same distal His in metNgb. [48] Distal helix residues, in addition to His81(E7), which exhibit significant dipolar shifts are Leu78(E4), Ala82(E8), Arg84(E10), Val85(E11), whose shifts are listed in Table 2. The chemical shifts for His81(E7) are given in Table 1, and data for the remaining assigned residues are provided in Supporting Information.

The two upfield hyperfine-shifted broad and strongly relaxed (T_1 ~ 3 ms) non-labile proton signals (Figures 2A, 2B) can only arise from the ligated His four ring non-labile protons. [34, 35, 44] The closest protons to the CHs of each of the two His are the His C_βHs (to the ring C_δH), and the ring N_δHs (to the ring C_εH). Saturation of the only clearly resolved peak at −9.5 ppm fails to exhibit (not shown) the sizable NOEs expected to His C_βHs if the peak arose from a C_δH, and hence identifies it as an axial His C_εH of one of the two His. The absence of a detectable NOE upon saturating this resolved His C_εH to the assigned His113(F8) N_δH peak at 18.4 ppm argues for its origin as the His81(E7) C_εH. In view of the very similar hyperfine shift pattern of the two axial His backbones, it is most likely that the other upfield broad and strongly relaxed resonances under the 2-vinyl H_βs arise from the C_εHs of His113(F8) (see below). The signals for the C_δHs of both axial His likely resonate in the broad composite peak (marked X) at ~15 ppm in Figure 2B.

Other sequence-specific assignments

Backbone connections (Figure 5) to the assigned Ala114(F9) trace over the FG loop and identify Leu115(FG1), His117(FG3) in contact with pyrrole C (Figure 1B), Val119(FG5) in contact with the junction of pyrrole B and C (Figure 1B), and the backbone in Lys116(FG2) and Lys118(FG4). A helical section represented by Val_m-AMX_{m+1}-AMX_{m+2}-$(N\alpha)_{m+3}$-Ile_{m+4}-Leu_{m+5}, with aromatic rings in contact with AMX_{m+1} and AMX_{m+2}, uniquely identifies Val122-Leu127, residues G3-G8 on the G helix. The expected NOESY cross peaks to pyrroles A and B are observed for Tyr123(G4), Phe124(G5) and Leu127(G8) (Figure 1B), and the C_ζH of Phe124(G5) exhibits the strong relaxation (T_1 ~20 ms) predicted by the crystal structure (R_{Fe} ~4.4 Å). Each of the residues exhibits significant dipolar shifts.

A short helical sequence Ala_n-$(N\alpha)_{n+1}$-$(N\alpha)_{n+2}$-AMX_{n+3}, the latter with contact to an aromatic ring, and with the Ala and the aromatic ring in contact with the junction of pyrroles B and C (Figure 1B), can only arise from Ala56(C4)-Tyr59(C7), with significant dipolar shifts exhibited by Ala56 and Tyr59. Backbone connections to Tyr59(C7) and a dipolar shifted, TOCSY-detected 2 spin aromatic ring in contact with the pyrrole B/C junction (Figure 1B), identifies Phe60(CD1). The failure to detect either TOCSY or NOESY connections between the C_εH signal and C_ζH of the ring argues for a C_ζH shift that is essentially degenerate with that of C_εHs.

Two short helical fragments, neither of whose side chains exhibits NOESY cross peaks to the heme, are represented by Val_p-$(N\alpha)_{p+1}$-Ala_{p+2}-$(N\alpha)_{p+3}$-AMX_{p+4}-Ala_{p+5} (with a four-spin aromatic ring in contact with AMX_{p+4}), and Ala_q-Z_{q+1}-$(N\alpha)_{q+2}$-Val_{q+3}-$(N\alpha)_{q+4}$-AMX_{q+5}-AMX_{q+6}, must arise from Val27-Ala32 and Ala44-Phe50 on helices A (A10-A15) and B (B8-B14). Aromatic rings in contact with the backbone of residue q+5 and q+6 confirm Phes at positions B13 and B14. The residues exhibit the expected NOESY cross peaks to other residues, as shown in Figure 1B. Only Leu46(B10) and Phe49(B13) exhibit significant dipolar shifts. Contacts to Trp131(A12) and Phe49(B13) identify two additional G-helices residues Val130 (G11) and Val135(G16). Resolution problems precluded unique identification of the H-helix, but expected (and observed) key contacts to the F and G helices (Figure 1B), together with unique TOCSY signals, identify Phe143(GH5)s, Trp151(H8), Val162(H19), Ala165(H22), Tyr166(H23) and Trp171(H28). Their position on the H-helix is confirmed by α_i-N_{i+3}/α_i-

β_{i+3} contact involving Val162(H19), Tyr159(H16) and Ala165(H22). The chemical shifts for residues with significant dipolar shifts (= 1 ppm for at least one proton) are listed in Table 2, and the remainder of the data is provided in Supporting Information.

Orientation and anisotropy of χ

The values of δ_{dip}(obs) obtained via Eq. (4) for all assigned residues with significant temperature dependence to their chemical shifts were used as input in the five parameter searches for $\Delta\chi_{ax}$, $\Delta\chi_{rh}$, α, β and κ = α + γ, using the two available sets of crystal coordinates for metCygb. [11, 12] In each case, very clear minima were observed with excellent correlation between δ_{dip}(obs) and δ_{dip}(calc) for the predicted five parameters, as illustrated in Figure 7A and 7B. The values for the optimized parameters are compared in Table 3. The alternate crystal coordinates yield values for the five parameters for the alternate crystal coordinates that are well within their uncertainties. The plot of δ_{dip}(obs) and δ_{dip}(calc) with sequence number, shown in Figures 8A and 8B, respectively, attest to the excellent definition of the nodal pattern through the structure. Figure 8C plots the temperature gradient of the chemical shift, d [δ_{DSS}(obs)]/d(T−1) versus sequence number. For the very few cases (marked by asterisk) where there appears to be a discrepancy between the signs of δ_{dip}(obs), and $\delta dip^{(calc),\ the}$ temperature gradient is found consistent with the sign of δ_{dip}(calc), indicating that the minor discrepancies between δ_{dip}(calc) and δ_{dip}(obs) in Figure 8A and 8B arises from the uncertainty in the calculated values of δ_{DSS}(dia).

Factoring the dipolar and contact shifts

The δ_{dip}(calc) for the heme and two axial His obtained by the alternate magnetic axes/ anisotropies in Table 3, are listed in Table 1, where the experimental δ_{hf} can be factored via Eq. (6) to yield δ_{con} for the heme methyl, meso-Hs and the two axial His. It is noted that the δ_{con} for the axial C_βHs and C_εH, which are dominated by the π-spin transfer into the highest bonding orbital of the imidazole ring, are indistinguishable for His81(E7) and His113(F8).

DISCUSSION

Active site solution molecular structure

The ^{1}H NMR data reveal the presence of predominantly a single ($\gtrsim$ 90%) molecular species. The fact that both Val119(FG5) and Phe60(CD1) make contact with pyrrole C (5-CH_3), and that both Val85(E11) and Ala88(E14) make contact with the heme at the junction of pyrroles A and D, dictate that the major isomer in solution has the heme orientation identified in the crystal structure, as depicted in Figure 1B, which is the same orientation as in mammalian globins, but corresponds to the minor isomer orientation of metNgb. [48] The two apparent heme methyl signals at 39.8 and 22.4 ppm in Figure 2A for a minor isomer (~10%) were too weak to detect the NOESY contacts required for detailed structural characterization. However, the pattern of the methyl shifts is that expected (and for metNgb observed [48]) for the isoelectronic, six-coordinate complex with the hemin rotated by 180° about the α-, γ-meso axis relative to that of the major isomer. The sequence-specific assignment of both the His81(E7) and His113 (F8) backbone in the major isomer, together with the expected, and demonstrated, moderate relaxation of the resolved $C_{\beta 2}$H signal for each ligand (as well as δ_{con}; see below) directly confirms that the distal His81(E7) is ligated to the iron in solution. Both the pattern of heme-residue and inter-residue NOESY cross peaks (summarized in Figure 1B), and the paramagnetically-induced relaxation, are consistent with the essentially indistinguishable active site molecular structure of the six-coordinated metCygb in the alternate crystal structures. [11, 12]

The ability to detect a significant population of an equilibrium, five-coordinate isomer with ruptured Fe-His(E7) bond, which would be high-spin and exhibit characteristic methyl signals

in the extreme low-field (~70–90 ppm) spectral window, depends on both the degree of population and the rate of the Fe-His(E7) bond scisson relative to the ^{1}H NMR methyl chemical shift difference.[50] We failed to detect by ^{1}H NMR in solution any hyperfine shifted resonances characteristic of a five-coordinate, high-spin metCygb complex [34] (if in slow exchange, [50] <1% population), and do not detect magnetization-transfer to an additional minor compound upon saturation of any of a number of resolved resonances for the major component in solution (if intermediate exchange [34, 50, 51]). Lastly, the temperature dependence in the heme methyl shifts for the dominant, low-spin isomer exhibit a behavior characteristic [34, 52] (see below) of a strongly dominant low-spin derivative, excluding the presence (<1%) of detectable five-coordinate, high-spin derivatives in the case of fast exchange. [34, 50] Hence we conclude that any equilibrium five-coordinate metCygb with the Fe-His(E7) bond ruptured must constitute <1% of the complex in solution.

Heme electronic structure

The heme methyl contact shift pattern, with large δ_{con} for 1-CH_3 and 5-CH_3, and small δ_{con} for 3-CH_3 and 8-CH_3, is similar to that reported33, 34 for mammalian metMbCN (although metCygb has a larger spread), with an orbital ground state where the lone unpaired spin is in the $3e_\pi(xz)$ molecular orbital. [53] Consistent with this ground state, and a nearby excited $3e_\pi(yz)$ state, the 5-CH_3 and 1-CH_3 δ_{con} exhibit strong Curie behavior (slope ~T^{-1}) in a plot of δ_{DSS}(obs) vs T^{-1}, while 3-CH_3 and 8-CH_3 exhibit anti-Curie (negative slope) behavior (not shown; see Supporting Information Figure 4S). [54, 55] It is noted that the pattern and spread of the heme methyl resonances in metCygb is very similar to that for the minor isomer of metNgb. [48] This pattern of methyl contact shifts and characteristic temperature dependence reflects[34, 52, 53] a molecular structure where the rhombic asymmetry is centered along the x′ axis in Figure 1A. Since the axial His (or Met) ligand is the primary source of the rhombic perturbation, the heme methyl contact shift pattern is consistent with a mean His imidazole plane orientation of the two His. The spread (but not the pattern) of the heme methyl shifts (~30 ppm) for metCygb is similar to that reported [56, 57] for the ferricytochrome b_5 with similar bis-His ligation, and several ferricytocheomes c. Comparison with the only other NMR characterized bis-His metglobins, those for the cyanobacteria *Synechoccus* [16, 58] and *Synechosistis* [18, 59] reveal a much smaller methyl shift spread (but the same pattern) for those globins than either metCygb or metNgb [48] and could be correlated with the mean of the two His imidazole planes [17] that deviate significantly from the x′ axis in Figure 1A.

Magnetic properties

The determination of the magnetic axes based on either set of crystal coordinates [11, 12] yields essentially the same values for the five parameters (Table 3) within the uncertainties. The axial anisotropy, 2.18×10^{-8} m^3/mol, and the rhombic anisotropy -0.49×10^{-8} m^3/mol are both ~20% smaller than found in metMbCN complexes, [34, 35] but are consistent with the anisotropies in bis-His ligated ferricytochromes b_5. 60, 61 The tilt of the major magnetic axes from the mean Fe-N_4 plane in metCygb is small (~5°). However, in each of the crystal structures, [11, 12] both Fe-N_ε(His) bonds are tilted from the mean N_4 plane by ~5°. For the WT metCygb crystal structure,[12] the 5° tilt in a direction ~120° with respect to x′, and corresponds remarkably to the (His(F8))N_ε-Fe-N_ε(His81(E7) vector, while in the C38S/C83S-metCygb structure, [11] the tilt and direction of tilt of z corresponds approximately to the FeN_ε (His113 (F8) vector. Thus the major magnetic axis is determined by the axial ligand bonds. The value of κ near zero for both magnetic axes determinations provides additional confirmation[52] of the comparable strength of the two His-Fe bonds, since κ ~0 is consistent with an effective rhombic perturbation that is precisely along the N_B-Fe-N_C vector, which, in turn, is the *mean* of the crystallographic His81(E7) (φ_{E7} = 25°) and His113(F8) (φ_{F8} = 22°) imidazole plane orientations, as depicted in Figure 1. If the His113(F8) bond were indeed much stronger than the His81(E7)-Fe bond, the Φ_{F8} ~20° would have lead to an expected κ ~20°.

It has been shown in a variety of metMbCN complexes[34, 62–64] that the pattern of meso-H hyperfine shifts is dominated by the rhombic anisotropy, and hence by κ. A value κ ~0 is directly supported by the meso-H shifts, as follows, where the parameter, $\Delta\delta_{meso}$; given by:

$$\Delta\delta_{meso}(\text{calc})=1/2[\,\delta_{DSS}(\alpha-\text{meso}-\text{H})-\delta_{DSS}(\beta-\text{meso}-\text{H}) +\delta_{DSS}(\gamma-\text{meso}-\text{H})-(\delta_{DSS}(\delta-\text{meso}-\text{H}))]=1.37\,\text{ppm}, \quad (6)$$

is consistent with the predicted value, $\Delta\delta_{meso}$(obs):

$$\Delta\delta_{meso}(\text{obs})=1/2[\,\delta_{dip}(\alpha-\text{meso}-\text{H})-\delta_{dip}(\beta-\text{meso}-\text{H})+\delta_{dip}(\gamma-\text{meso}-\text{H})- \delta_{dip}(\delta-\text{meso}-\text{H})]=0.2\pm3.2\text{ and }1.0\pm3.4\,\text{ppm} \quad (7)$$

for the magnetic axes deterined on the basis of the WT metCygb and C38S/C83S-metCygb crystal structures, respectively.

The nature of the axial His-Fe interaction

Factoring $^{\delta}$hf into δ_{con} and δ_{dip} for the two magnetic axes determinations lead to indistinguishable imidazole $C_{\varepsilon}H$ contact shifts of 27±4 ppm and $C_{\beta 2}H$ contact shifts 6.8±1.3 ppm. The His δ_{con} pattern for both His are very similar to those obtained for either cyanomet myoglobins[35] or ferricytochromes, [36] and reflect imidazole to iron π-spin transfer that leads to large upfield δ_{con} for $C_{\varepsilon}H$, significant low-field δ_{con} for the $C_{\beta}H$. $\delta_{con}(C_{\varepsilon}H)$ is directly proportional to π-spin density, while the relation between the His $C_{\beta}H$ contact shift and the C_{γ} π-spin density depends on the C_{γ}-C_{β}-H dihedral angle, Ψ, 34, 65with the imidazole plane. The crystal structures reveal the same Ψ ~56±2° for the two His $C_{\beta 2}H$, such that the π-spin densities for C_{γ} of the two axial His are also indistinguishable. The Ψ ~16±10 for $C_{\beta 1}H$ of the two axial His predict much smaller δ_{con} for $C_{\beta 1}H$ than $C_{\beta 2}H$, as observed in Table 1. The indistinguishable π-spin densities on the two His rings dictate very similar Fe-His covalency, and hence similar bond strengths.

CONCLUSIONS

Two important conclusion follow from the present work; 1) solution ^{1}H NMR of the paramagnetic six-coordinate metglobins can be effectively utilized to determine the relative covalencies of the two axial His-Fe bonds; and 2) human metcytoglobin, in solution, detectably populates only six-coordinate metCygb for which the bond strength of Fe-imidazole for the proximal and distal His are essentially indistinguishable. Thus the ^{1}H NMR results argue against significant strain in the Fe-His(E7) relative to the Fe-His(F8) bond as the basis for the greater lability of the distal His(E7) required for exogenous ligand binding. The possibility that there is strain, or reduced dynamic stability, of the distal helix in metCygb relative to conventional, five-coordinate, metMb, as reflected in the rate of backbone NH exchange, [66] is under study.

Supplementary Material

Refer to Web version on PubMed Central for supplementary material.

Acknowledgements

This research was supported by grants from the National Institutes of Health, HL 16087 (GNL), and European Union project “Neuroglobin and the survival of the neuron QLRT; 2001-01548 (L.M.), S.D. is a postdoctoral fellow of the Fund for Scientific Research-Flanders.

References

1. ABBREVIATIONS: DSS, 2,2-dimethyl-2-silapentane-5-sulfonate; DMDH, 2-, 4-dimethyldeuterohemin; PH, protohemin, NOESY, two-dimensional nuclear Overhauser spectroscopy; TOCSY, two-dimensional total correlation spectroscopy; HO, heme oxygenase; *Nm*HO, *Neisseria meningitidis; Nm*HO-DMDH-CN, *Neisseria meningitidis* heme oxygenase-2-,4-dimethyldeuterohemin-cyanide; *Nm*HO-PH-CN, *Neisseria meningitidis* heme oxygenase-protohemin-cyanide; MALDI-TOF, matrix-assisted laser desorption ionization -time of flight.
2. Antonini, E.; Brunori, M. Hemoglobin and Myoglobin and Their Reactions with Ligands. Elsevier, North-Holland Publishing; Amsterdam: 1971.
3. Dickerson, RE.; Geis, I. Hemoglobin: Structure, Function, Evolution and Pathology. Benjamin-Cummings; Menlo Park, CA: 1983.
4. Perutz MF, Wilkinson AJ, Paoli M, Dodson GG. Ann Rev Biophys 1998;27:1–34.
5. Wittenberg JB, Bolognesi M, Wittenberg BA, Guertin M. J Biol Chem 2002;277:871–874. [PubMed: 11696555]
6. Ouellet H, Ouellet Y, Richard C, Labarre M, Wittenberg B, Wittenberg J, Guertin M. Proc Natl Acad Sci (USA) 2002;99:5902–5907. [PubMed: 11959913]
7. Milani M, Savard PY, Ouellet H, Ascenzi P, Guertin M, Bolognesi M. Proc Natl Acad Sci 2003;100:5766–5771. [PubMed: 12719529]
8. Milani M, Pesce A, Ouellet Y, Dewilde S, Friedman JM, Ascenzi P, Guertin M, Bolognesi M. J Biol Chem 2004;279:21520–21525. [PubMed: 15016811]
9. Milani M, Pesce A, Nardini M, Ouellet H, Ouellet Y, Dewilde S, Bocedi A, Ascenzi P, Guertin M, Moens L, Friedman JM, Wittenberg JB, Bolognesi M. J Inorg Biochem 2005;99:97–109. [PubMed: 15598494]
10. Hargrove MS, Brucker EA, Stec B, Sarath G, Arredondo-Peter R, Klucas RV, Olson JS, Phillips GNJ. Structure 2000;8:1005–1014. [PubMed: 10986467]
11. de Sanctis D, Dewilde S, Pesce A, Moens L, Ascenzi P, Hankeln T, Burmester T, Bolognesi M. J Mol Biol 2004;336:917–927. [PubMed: 15095869]
12. Sugimoto H, Makino M, Sawai H, Kawada N, Yoshizato K, Sshiro Y. J Mol Biol 2004;339:873–885. [PubMed: 15165856]
13. de Sanctis D, Dewilde S, Vonrhein C, Pesce A, Moens L, Ascenzi P, Hankeln T, Burmester T, Ponassi M, Nardini M, Bolognesi M. J Biol Chem 2005;280:27222–27229. [PubMed: 15917230]
14. Pesce A, Dewilde S, Nardini M, Moens L, Ascenzi P, Hankeln T, Burmester T, Bolognesi M. Structure 2003;11:1087–1095. [PubMed: 12962627]
15. Vallone B, Nienhaus K, Brunori M, Nienhaus GU. Proteins: Struct, Funct, Bioinf 2004;56:85–92.
16. Scott NL, Falzone CJ, Vuletich DA, Zhao J, Bryant DA, Lecomte JTJ. Biochemistry 2002;41:6902–6910. [PubMed: 12033922]
17. Hoy JA, Kundu S, Trent JTI, Ramaswamy S, Hargrove MS. J Biol Chem 2004;279:16535–16542. [PubMed: 14736872]
18. Lecomte JTJ, Scott NL, Vu C, Falzone CJ. Biochemistry 2001;40:6541–6552. [PubMed: 11371218]
19. Vallone B, Nienhaus K, Matthes A, Brunori M, Neinhaus GU. Proc Natl Acad Sci (USA) 2004;101:17351–17356. [PubMed: 15548613]
20. Dewilde S, Kiger L, Burmester T, Hankeln T, Baudin-Creuza V, Aerts T, Marden MC, Caubergs R, Moens L. J Biol Chem 2001;276:38949–38955. [PubMed: 11473128]
21. Trent JTI, Hvitved AN, Hargrove MS. Biochemistry 2001;40:6155–6163. [PubMed: 11352753]
22. Burmester T, Weich B, Reinhardt S, Hankeln T. Nature 2000;407:520–523. [PubMed: 11029004]
23. Burmester T, Ebner B, Weich B, Hankeln T. Mol Biol Evol 2002;19:416–421. [PubMed: 11919282]
24. Trent JTI, Hargrove MS. J Biol Chem 2002;277:19538–19545. [PubMed: 11893755]
25. Kawada N, Kristensen DB, Asahina K, Nakatani K, Minamiyama Y, Seki S, Yoshizato K. J Biol Chem 2001;276:25318–25323. [PubMed: 11320098]
26. Pesce A, Bolognesi M, Bocedi A, Dewilde S, Moens L, Hankeln T, Burmester T. EMBO Rep 2002;3:1146–1151. [PubMed: 12475928]

27. Hankeln T, Ebner B, Fuchs C, Gerlach F, Haberkamp M, Laufs TL, Roesner A, Schmidt M, Weich B, Wystub S, Saaler-Reinhardt S, Reuss S, Bolognesi M, Sanctis DD, Marden MC, Kiger L, Moens L, Dewilde S, Nevo E, Avivi A, Weber RE, Fago A, Burmester T. J Inorg Biochem 2005;99:110–119. [PubMed: 15598495]
28. Couture M, Burmester T, Hankeln T, Rousseau DL. J Biol Chem 2001;276:36377–36382. [PubMed: 11473111]
29. Hamdane D, Kiger L, Dewilde S, Green BN, Pesce A, Uzan J, Burmester T, Hankeln T, Bolognesi M, Moens L, Marden MC. J Biol Chem 2003;278:51713–51721. [PubMed: 14530264]
30. Spiro, TG. Resonance Raman Spectroscopy of Hemes and Hemoproteins. Wiley-Interscience; New York: 1988.
31. Sawai H, Makino M, Mizutani Y, Ohta T, Sugimoto H, Uno T, Kawada N, Yoshizato K, Kitagawa T, Shiro Y. Biochemistry 2005;44:13257–13265. [PubMed: 16201751]
32. Sawai H, Kawada N, Yoshizato K, Nakajima H, Aono S, Shiro Y. Biochemistry 2003;42:5133–5142. [PubMed: 12718557]
33. Bertini I, Turano P, Vila AJ. Chem Rev 1993;93:2833–2933.
34. La Mar, GN.; Satterlee, JD.; de Ropp, JS. The Porphyrins Handbook. Kadish, KM.; Smith, KM.; Guilard, R., editors. 5. Academic Press; San Diego: 2000. p. 185-298.
35. Nguyen BD, Xia Z, Yeh DC, Vyas K, Deaguero H, La Mar G. J Am Chem Soc 1999;121:208–217.
36. Brennan L, Turner DL. Biochim Biophys Acta 1997;1342:1–12. [PubMed: 9366264]
37. La Mar GN, de Ropp JS. Biol Magn Reson 1993;18:1–79.
38. Bertini, I. The Porphryins. Kadish, KM.; Smith, KM.; Guilard, R., editors. Academic Press; New York: 2000.
39. Williams G, Clayden NJ, Moore GR, Williams RJP. J Mol Biol 1985;183:447–460. [PubMed: 2991533]
40. Emerson SD, La Mar GN. Biochemistry 1990;29:1556–1566. [PubMed: 2334714]
41. Gupta RK. J Magn Reson 1976;24:461–465.
42. Jeener J, Meier BH, Bachmann P, Ernst RR. J Chem Phys 1979;71:4546–4553.
43. Griesinger C, Otting G, Wüthrich K, Ernst RR. J Am Chem Soc 1988;110:7870–7872.
44. Emerson SD, La Mar GN. Biochemistry 1990;29:1545–1555. [PubMed: 2334713]
45. Neal S, Nip AM, Zhang H, Wishart DS. J Biomol NMR 2003;26:215–240. [PubMed: 12766419]
46. Cross KJ, Wright PE. J Magn Reson 1985;64:220–231.
47. Thériault Y, Pochapsky TC, Dalvit C, Chiu ML, Sligar SG, Wright PE. J Biomol NMR 1994;4:491–504. [PubMed: 8075538]
48. Du W, Syvitski RT, Dewilde S, Moens L, La Mar GN. J Am Chem Soc 2003;125:8080–8081. [PubMed: 12837059]
49. Wüthrich, K. NMR of Proteins and Nucleic Acids. Wiley & Sons; New York: 1986.
50. Sandström, J. Dynamic NMR Spectroscopy. Academic Press; New York: 1982.
51. Qin J, Pande U, La Mar GN, Ascoli F, Ascenzi P, Cutruzzola F, Travaglini Allocatelli C, Brunori M. J Biol Chem 1993;278:4012–4021.
52. Shokhirev NV, Walker FA. J Biol Inorg Chem 1998;3:581–594.
53. Walker, FA. The Porphyrin Handbook. Kadish, KM.; Smith, KM.; Guilard, R., editors. 5. Academic Press; Boston: 2000. p. 1-183.
54. Turner DL. Eur J Biochem 1993;211:563–568. [PubMed: 8382155]
55. Shokhirev NV, Walker FA. J Phys Chem 1995;99:17795–17804.
56. Keller RM, Wüthrich K. Biochim Biophys Acta 1980;621:204–217. [PubMed: 7353039]
57. La Mar GN, Burns PD, Jackson JT, Smith KM, Langry KC, Strittmatter P. J Biol Chem 1981;256:6075–6079. [PubMed: 7240191]
58. Falzone CJ, Kao YH, Zhao J, Bryant DA, Lecomte JTJ. Biochemistry 1994;33:6052–6062. [PubMed: 8193119]
59. Falzone CJ, Vu BC, Scott NL, Lecomte JTJ. J Mol Biol 2002;325:1015–1029. [PubMed: 12470956]
60. Banci L, Pierattelli R, Turner DL. Eur J Biochem 1995;232:522–527. [PubMed: 7556202]

61. Arnesano F, Banci L, Bertini I, Felli IC. Biochemistry 1998;37:173–184. [PubMed: 9425037]
62. Wu Y, Chien EYT, Sligar SG, La Mar GN. Biochemistry 1998;37:6979–6990. [PubMed: 9578585]
63. Xia Z, Zhang W, Nguyen BD, Kloek AP, Goldberg DE, La Mar GN. J Biol Chem 1999;274:31819–31826. [PubMed: 10542205]
64. Du W, Xia Z, Dewilde S, Moens L, La mar GN. Eur J Biochem 2003;270:2707–2720. [PubMed: 12823541]
65. Bertini I, Luchinat C. Coord Chem Rev 1996;150:1–296.
66. Englander SW, Kallenbach NR. Quart Rev Biophys 1984;16:521–655.

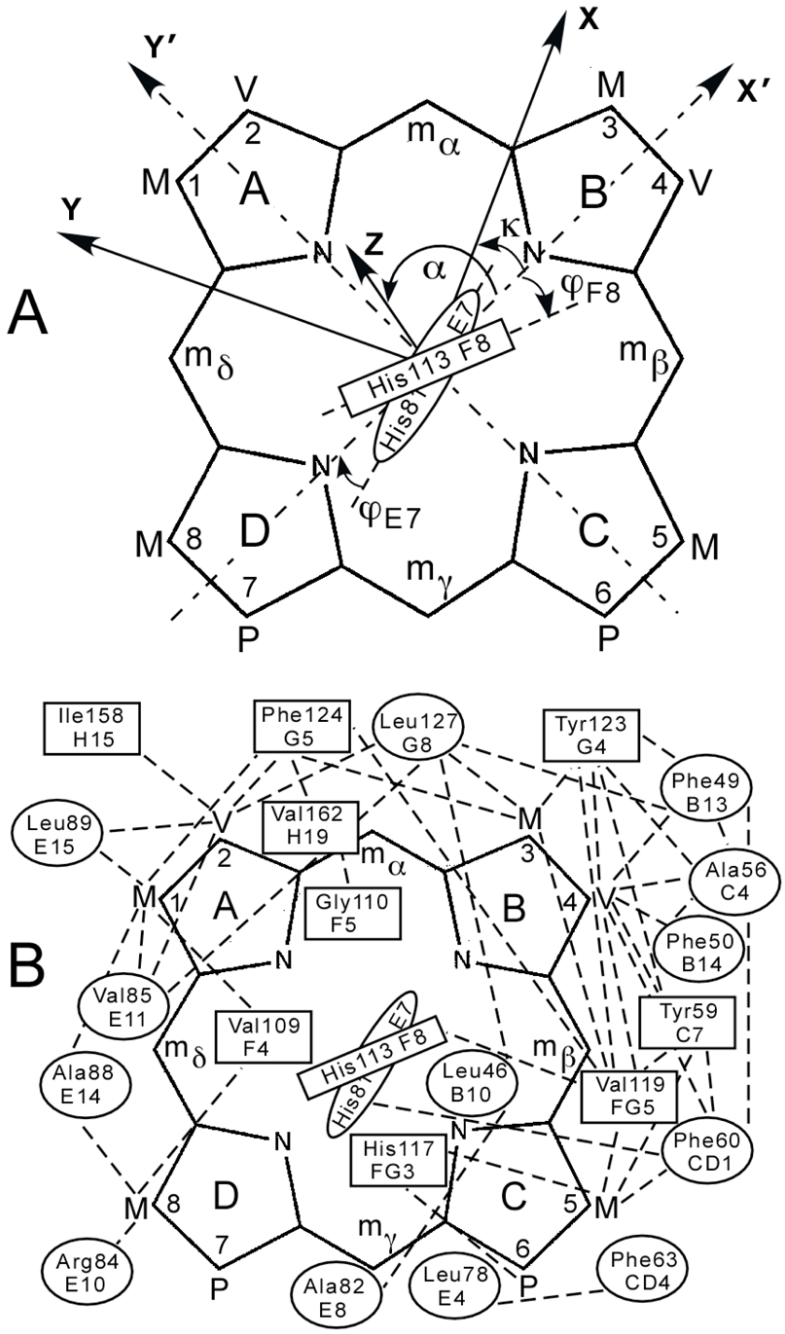

Figure 1.

(**A**) Reference coordinate system, x′, y′, z′, with x′, y′ in the heme plane and z′ normal to the heme. The magnetic coordinate system, x, y, z, with β, the tilt of the major magnetic axis, z, from the heme normal, z′, α, indicates the direction of the tilt given by the projection of z onto the x′, y′ plane and the x′ axis, and κ ~ α + γ, locates the rhombic axes. The two angles, ϕ_{F8} and ϕ_{E7}, represent the orientation of the His113(F8) and His81(E7) imidazole planes, respectively, relative to the x′ axis. (**B**) Schematic representation of the heme pocket of metCygb (squares are proximal residues and circles are distal). The observed (and expected) NOESY connections between the heme substituents and heme pocket residues, and between

heme pocket residues of different helixes (or loops) are shown by dashed lines. Residues are labeled by residue type, residue number and helical (or loop) positions in the standard Mb fold.

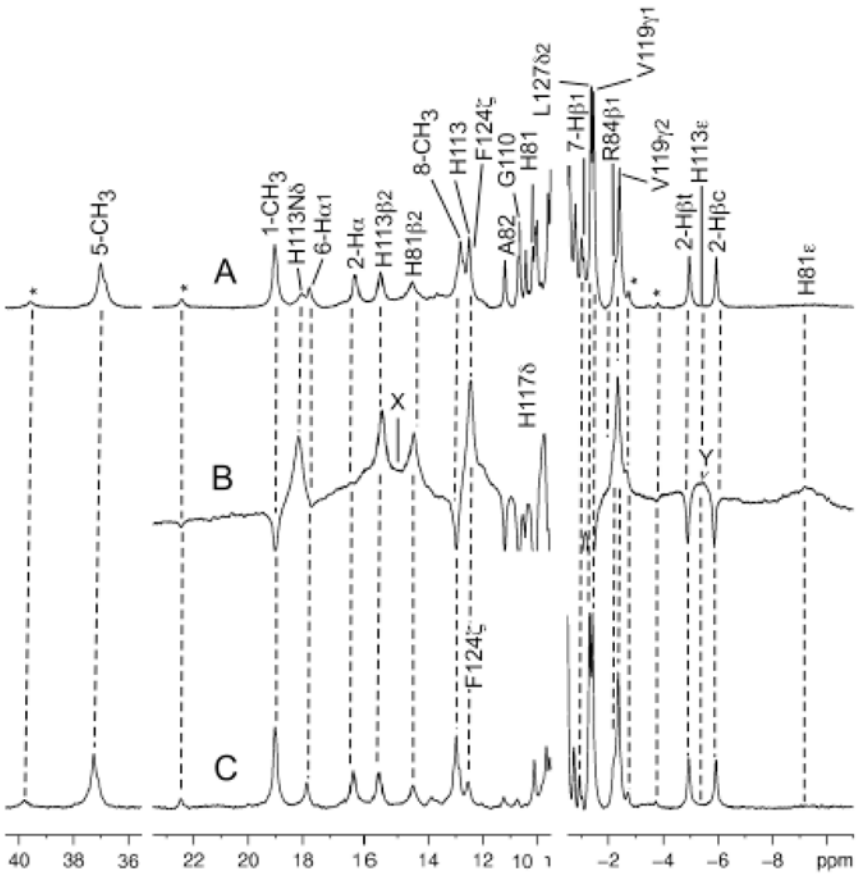

Figure 2.

Resolved portions of the ^{1}H NMR spectra of human metCygb, 50 mM in phosphate, pH 7.5 at 25°C. Heme signals are identified by the Fischer notation (Figure 1) and residue peaks are labeled by residue type, residue number and proton position, (**A**) the 600 MHz slow repetition rate (1 s^{-1}) reference spectrum in $^{1}H_2O$; (**B**) the 500 MHz WEFT-spectrum (repetition rate 5 s^{-1}, relaxation delay 40 ms), which emphasizes the moderately to strongly relaxed protons; (**C**) the 500 MHz slow-repetition rate (1 s^{-1}) reference spectrum in $^{2}H_2O$.

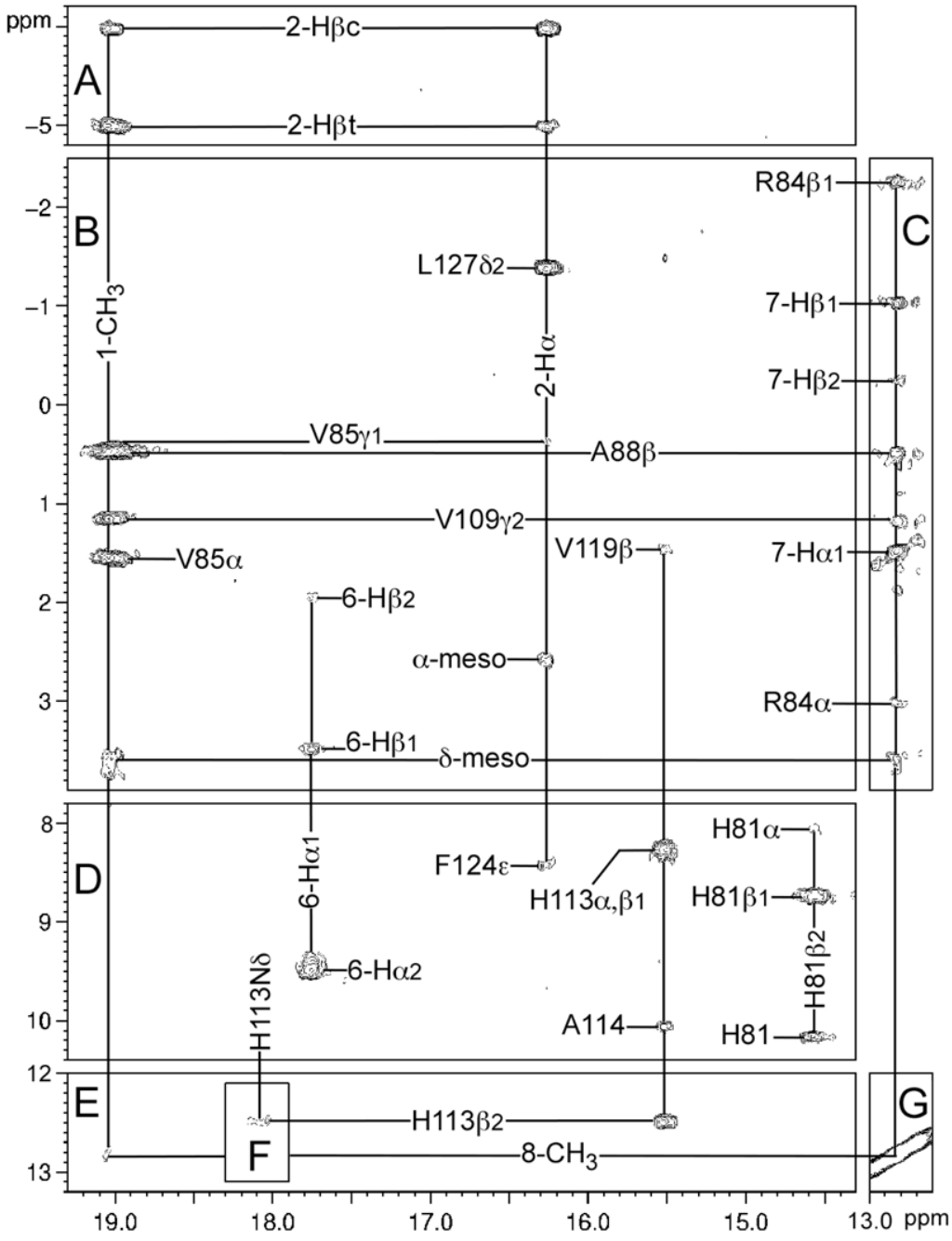

Figure 3.

Portions of the 600 MHz ^{1}H NMR NOESY spectrum of metCygb in ^1H_2O, 50 mM in phosphate, pH 7.5 at 25°C (repetition rate 1 s^{-1}, mixing time 60 ms), illustrating intra-heme key contacts: 1-CH_3 to (**E**) 8-CH_3, (**A**) 2-H_βs, (**B**) the δ-meso; 8-CH_3 to (**C**) 7-propinate and the δ-meso; (**A**) intra-2-vinyl and (**B**) 2-H_α to the α-meso; (**B, D**) intra-6-propinate as well as (**D**) intra-His81(E7) and (**D**, **E**) intra-His113(F8) connections, His113(F8) to (**D**) Ala114(F9) and to (**B**) Val119(FG5) contacts. Also shown are contacts that establish heme orientation: (**B**) 1-CH_3 to Val85(E11), Ala88(E14) and Val109(F4), 2-H_α to Val85(E11), (**C**) 8-CH_3 to Arg84(E10), Ala88(E14) and Val109(F4). The cross-peak between His113(F8) NH and NδH

in Section **F** is shown with lower levels (by factor of 1.5) of 60° shifted-sine-squared-bell apodization of the NOESY spectrum.

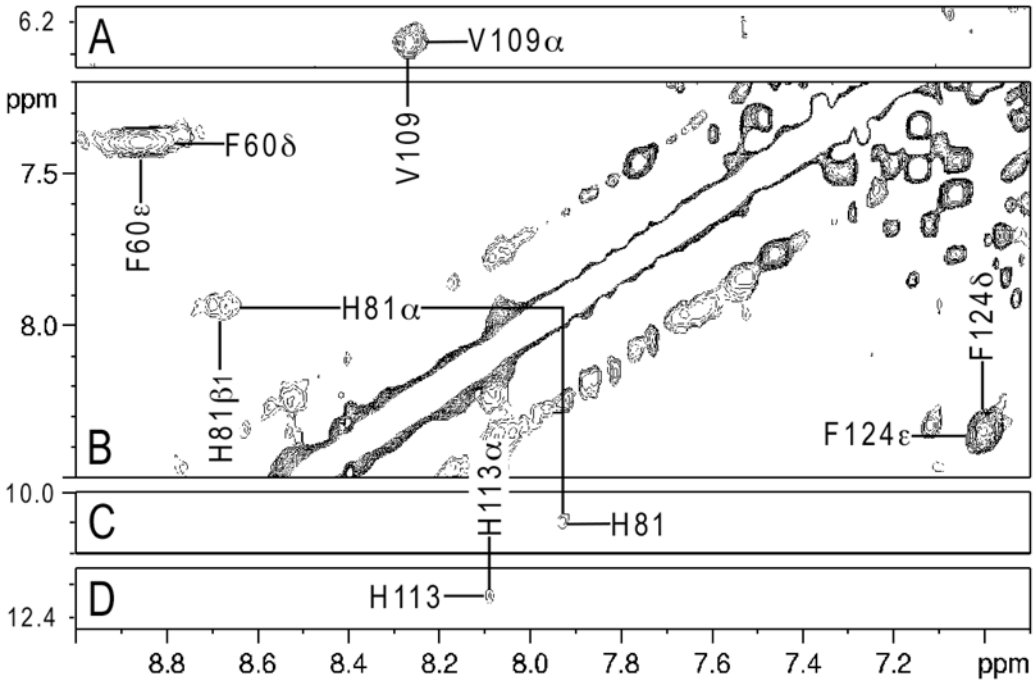

Figure 4.

Portion of the 500 MHz ^{1}H NMR clean-TOCSY spectrum of metCygb in ^1H_2O, 50 mM in phosphate, pH 7.5 at 30°C (repetition rate 1 s^{-1}, mixing time 25 ms) illustrating scalar connections for the moderately relaxed $C_\beta H$-$C_\alpha H$-NH of His81(E7), $C_\alpha H$-NH of His113(F8), Val109(F4) and the rings of Phe60(CD1) and Phe124(G5).

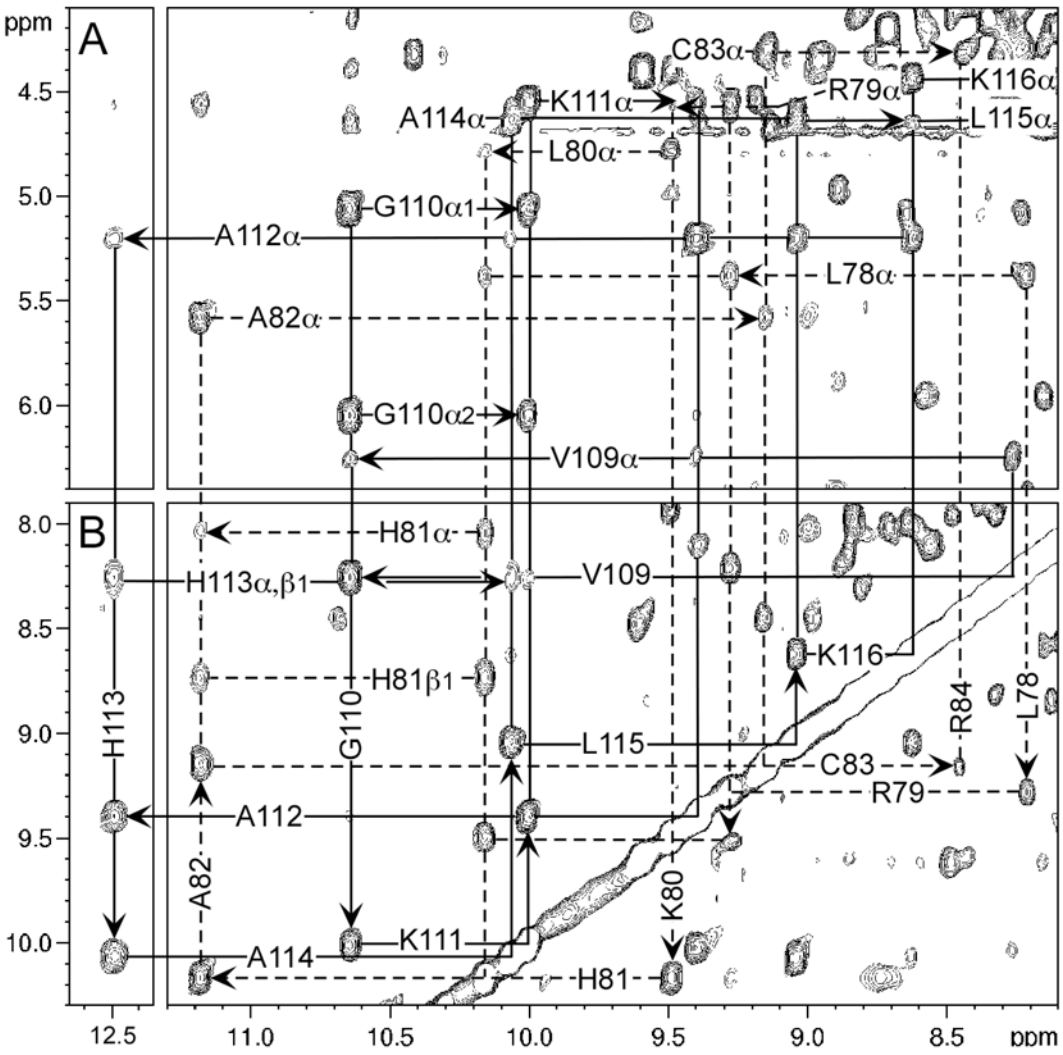

Figure 5.

Fingerprint region of the 600 MHz ^{1}H NMR NOESY spectrum of metCygb in $^{1}H_2O$, 50 mM in phosphate at 25°C (repetition rate 1 s^{-1}, mixing time 60 ms), illustrating the characteristic helical N_i-N_{i+1} connection for the (**A**, **B**) proximal helix (i = F4-FG1 (Val109-Leu115); upper left of diagonal in (**B**), solid), and (**B**) the distal helix (i = E4-E9 (Leu78-Cys83); lower right of diagonal, dash) and signature α_i-N_{i+1} connection for (**A**, **B**) the proximal (solid) and distal (dash) residues.

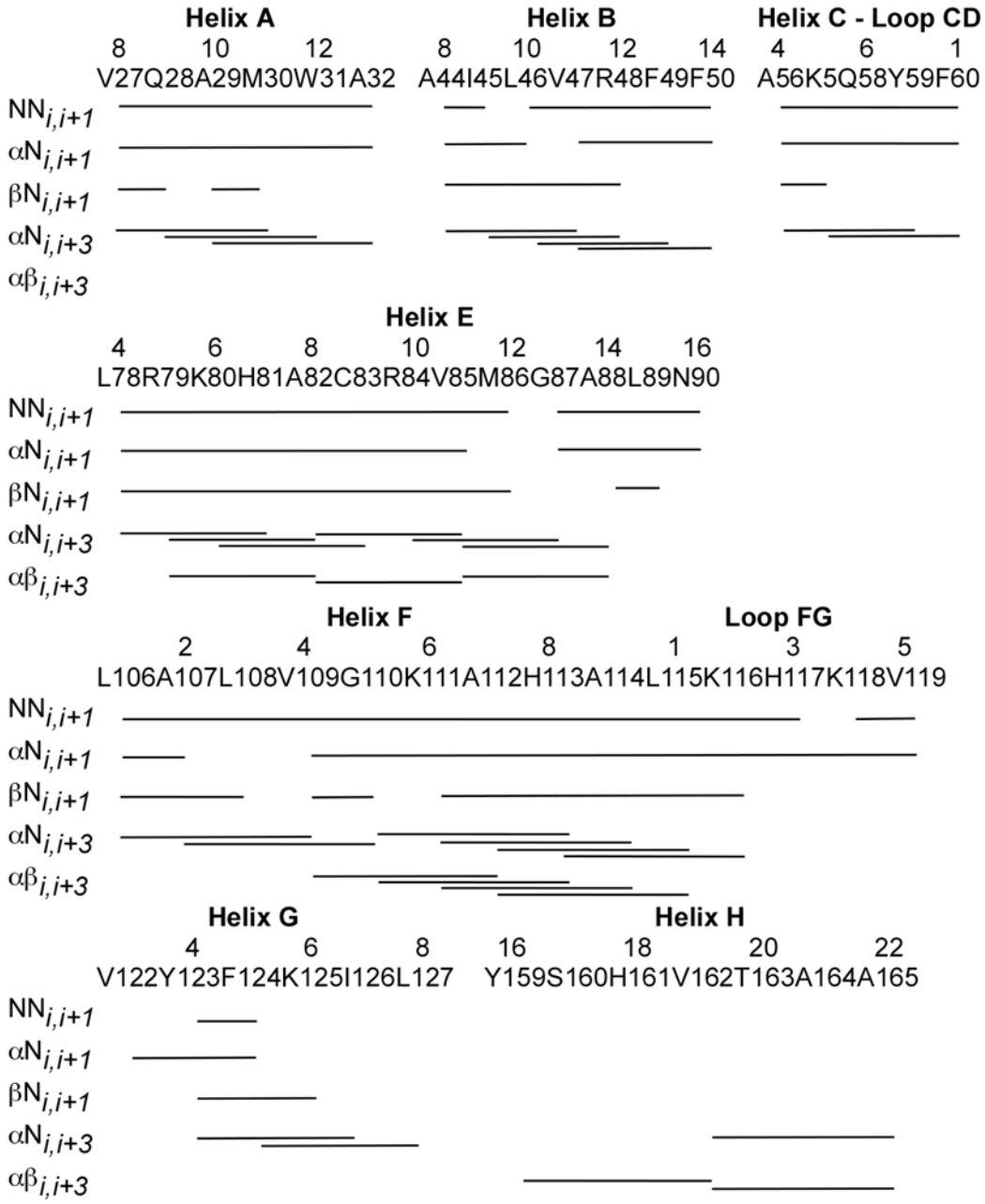

Figure 6.
Schematic depiction of the observed characteristic backbone NOESY connection that provided the assignment of seven helices and two inter-helical loops. Helixes and loops (the first and second lines) refer to those in vertebrate globins.

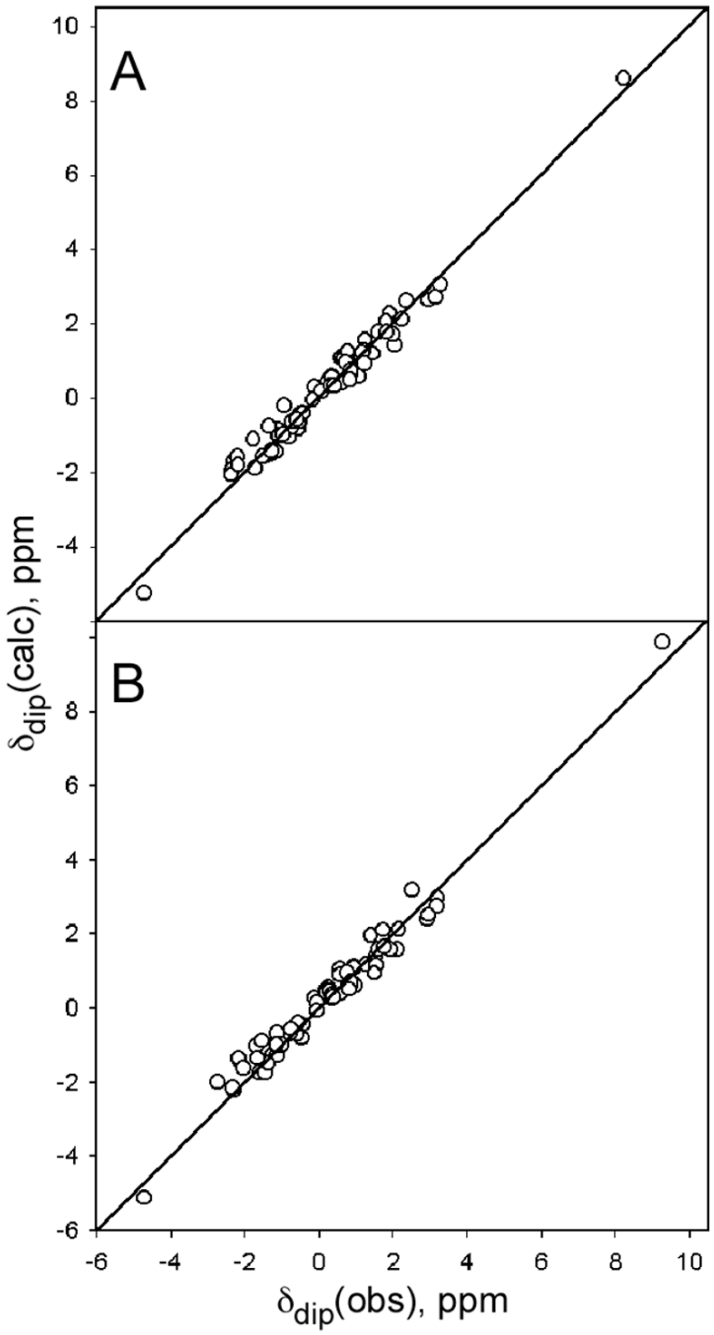

Figure 7.

Plot of δ_{dip}(obs) versus δ_{dip}(calc) for the optimized anisotropies and orientation of the paramagnetic susceptibility tensor χ when using the crystal coordinates of (**A**) C38S/C83S-metCygb: $\Delta\chi_{ax} = 2.18 \times 10^{-8}$ m^3/mol; $\Delta\chi_{rh} = -0.52 \times 10^{-8}$ m^3/mol; $\alpha = 80$; $\beta = 6$; $\kappa = -4$, F/n = 0.10[11] and (**B**) WT metCygb: $\Delta\chi_{ax} = 2.08 \times 10^{-8}$ m^3/mol; $\Delta\chi_{rh} = -0.49 \times 10^{-8}$ m^3/mol, $\alpha = 120°$, $\beta = 5°$, $\kappa = 0°$, F/n = 0.11[12] to evaluate the geometric factors in Eq. (2). Protons whose δ_{dip}(obs) were used for the calculations are labeled in Table 1S (Supporting Information).

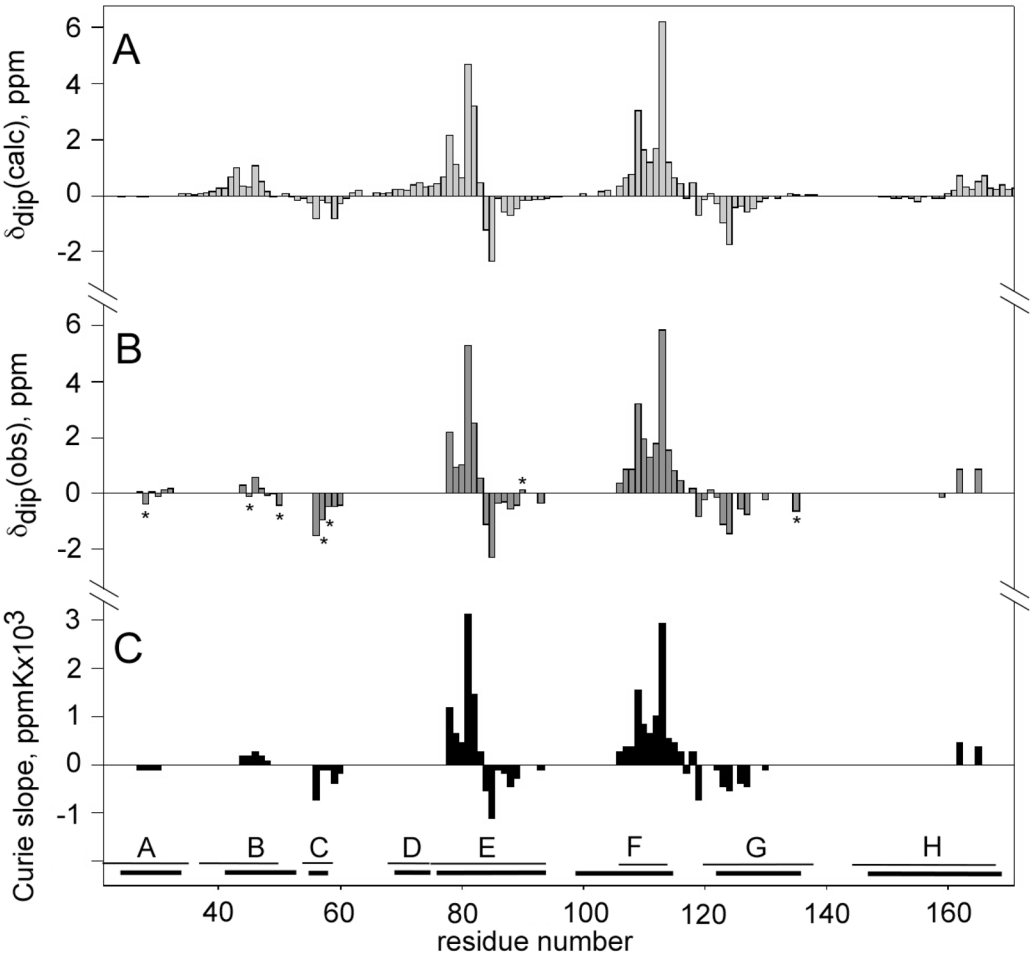

Figure 8.

Plot of the backbone metCygb $C_\alpha H$ (**A**) δ_{dip}(calc), (**B**) δ_{dip}(obs) for optimized magnetic axes depicted in Figure 7B and Table 3, and (**C**) the observed Curie slope, d[δ_{DSS}(obs)]/d[1/T], each versus residue numbers for the residues detected in the crystal structure. The positions of helices are shown at the bottom for Mb (thin lines) and Cygb (thick lines).

Table 1

Observed chemical shifts, dipolar shifts and contact shifts for the heme and two axial His ligands in human metcytoglobin

Heme	δ_{DSS}(obs)[a](T_1)[b]	δ_{DSS}(dia)[c]	δhf[d]	δ_{dip}(calc)[e]	δ_{con}[f]	δ_{dip}(calc)[g]	δ_{con}[f]
1-CH_3	18.81(105)	3.6±0.2	15.2±0.2	−2.5±0.2	17.7±0.4	−2.9±0.3	18.1±0.5
3-CH_3	6.59	3.8±0.2	2.8±0.2	−4.7±0.4	7.5±0.6	−5.0±0.5	7.8±0.7
5-CH_3	36.43 (95)	2.5±0.3	33.9±0.3	−2.5±0.2	36.4±0.5	−2.9±0.3	36.8±0.6
8-CH_3	13.29 (105)	3.6±0.2	9.7±0.2	−4.3±0.4	14.0±0.6	−5.2±0.5	14.9±0.7
6-C_αHs	17.61(90), 9.68						
6-C_βHs	3.41, 1.92						
7-C_αHs	2.05, 2.05						
7-C_βHs	−0.92, −0.07						
2H_α	16.23 (85)						
2H_βs	−4.76, −5.67(150)						
4H_α	5.22						
4H_βs	−0.23, −0.71						
α-meso-H[h]	2.86	9.9±0.5	−7.0±0.5	−9.8±0.8	2.8±1.3	−9.9±0.8	2.9±1.3
β-meso-H[h]	1.50	9.3±0.5	−7.8±0.5	−9.6±0.8	1.8±1.3	−10.9±0.9	3.1±1.4
γ-meso-H[h]	5.37	10.2±0.4	−4.8±0.4	−9.8±0.8	5.0±1.2	−9.9±0.8	5.1±1.2
δ-meso-H[h]	3.98	9.9±0.4	−5.9±0.4	−9.6±08	3.7±1.2	−10.9±0.9	5.0±1.3
His81(E7)[i]							
[E6][k]							
NH	10.06	7.8±0.4	2.8±0.4	2.4±0.2	0.4±0.6	2.4±0.2	0.4±0.6
C_αH	7.88	2.7±0.2	5.2±0.2	4.6±0.4	0.6±0.6	4.2±0.4	1.0±0.6
$C_{\beta1}$ H	8.65	1.9±0.3	6.8±0.3	6.7±0.6	0.1±0.9	6.2±0.5	0.6±0.8
$C_{\beta2}$ H	14.24(49)	1.8±0.3	12.4±0.3	6.1±0.5	6.3±0.8	6.3±0.5	6.0±0.8
C_εH	−8.7 (~3)	2.3±1.0	−11±1.0	19.6±1.6	−30.7±2.6	15.2±1.3	−26±2.3
C_δH	15±2(~3)	0.0±0.7	15±2.7	14.3±1.2	−0.7±3.9	19.9±1.6	−4.9±4.3
His113(F8)[i]							
[F15] $_k$							
NH	12.31	7.1±0.4	5.9±0.4	5.2±0.4	0.7±0.8	6.3±0.5	−0.4±0.9
C_αH	8.10	2.2±0.2	5.7±0.2	6.2±0.5	−0.5±0.7	6.8±0.6	−1.1±0.8
$C_{\beta1}$ H	8.10	1.5±0.3	7.2±0.3	6.2±0.5	1.0±0.8	6.5±0.6	0.7±0.9
$C_{\beta2}$ H	15.2(47)	1.7±0.3	14.4±0.3	6.9±0.6	7.5±0.9	7.5±0.6	6.9±0.9
C_εH	−4.95(~3)	0.8±0.8	−5.8±0.8	17.6±1.4	−23.4±2.2	22.2±1.8	−28.0±2.6
C_δH	15±2(~3)	−0.8±0.7	15.8±2.7	15.7±1.3	0.1±4.0	11.5±1.0	4.3±3.7
N_δH	18.4(20)	7.4±0.4	11.0±0.4	12.2±1.0	1.2±1.4	14.2±1.2	−3.2±1.6

[a] Observed chemical shift, in ppm, from DSS, in ^1H_2O, 50 mM in phosphate, pH 7.5 at 30°C.

[b] T_1, in ms, for resolved resonances.

[c] Chemical shift for an isostructural diamagnetic complex, as provided by the shift X [45] and the porphyrin ring current [46] program. For the heme methyls and meso-protons of the cytoglobin the chemical shifts for MbCO [47] were used.

[d] Experimental hyperfine shift (Eq. (1)), as obtained from δ_{DSS}(obs) − δ_{DSS}(dia).

[e] Dipolar shift, as calculated by the optimized magnetic axes described in Table 3 and Figure 7. Magnetic axes were obtained using WT metCygb crystal coordinates. [12].

[f] Contact shift, as obtained from Eq. (1) and Eq. (2).

[g] Dipolar shift, as calculated by the optimized magnetic axes described in Table 3 and Figure 7. Magnetic axes were obtained using C38S/C83S metCygb crystal coordinates for chain B.[11]

[h] All the meso protons were artificially placed with the same distance from the Fe ion when their dipolar shift was calculated.

[i] Helical/loop position in mammalian (i.e., axial His is F8, distal is E7, etc) Mb fold is given in parenthesis.

[k] Actual helical/loop positions in Cygb are given in square brackets.

Table 2

Chemical shifts for strongly dipolar shifted residues in metCygb.[a]

Residue	Proton	δ_{DSS}(obs)
Leu46(B10)[e] [B6][f]	NH	8.44
	$C_\alpha H$	4.12
	$C_\beta Hs$[b]	2.45, 2.85
	$C_\gamma H$	3.22
	$C_\delta H_3 s$[b]	2.98, 1.75
Phe49(B13)[e] [B9][f]	NH	8.14
	$C_\alpha H$	4.30
	$C_\beta Hs$	3.18, 2.70
	$C_\delta Hs$	5.98
	$C_\varepsilon Hs$	5.74
	$C_\zeta H$	5.57
Ala56(C4)[e] [C3][f]	NH	7.99
	$C_\alpha H$	2.87
	$C_\beta H_3$	0.38
Tyr59(C7)[e] [CD2][f]	NH	5.56
	$C_\alpha H$	3.70
	$C_\beta Hs$[b]	0.72, 1.77
	$C_\delta Hs$	6.27
	$C_\varepsilon Hs$	6.11
Phe60(CD1)[e] [CD3][f]	NH	7.46
	$C_\alpha H$	4.37
	$C_\delta Hs$	7.39
	$C_\varepsilon Hs$	8.83
Leu78(E4)[e] [E3][f]	NH	8.17
	$C_\alpha H$	5.31
	$C_\beta Hs$[b]	1.45, 2.37
	$C_\gamma H$	2.40
	$C_\delta H_3 s$[b]	1.55, 0.82
Ala82(E8)[e] [E7][f]	NH	11.07
	$C_\alpha H$	5.48
	$C_\beta H_3$	2.44
Arg84(E10)[e] [E9][f]	NH	8.42
	$C_\alpha H$	3.08
	$C_\beta Hs$[b]	−2.12(55),[c] 0.61
	$C_\gamma Hs$	0.91, 1.30(?)[d]
Val85(E11)[e] [E10][f]	NH	8.93
	$C_\alpha H$	1.62
	$C_\beta H$	2.79
	$C_\gamma H_3 s$[b]	0.38, 2.08(?)[d]
Ala88(E14)[e] [E13][f]	NH	6.88
	$C_\alpha H$	3.79
	$C_\beta H_3$	0.52
Val109(F4)[e] [F11][f]	NH	8.24
	$C_\alpha H$	6.13
	$C_\beta H$	3.47
	$C_\gamma H_3$[b]	4.02, 1.14
Gly110(F5)[e] [F12][f]	NH	10.58
	$C_\alpha Hs$[b]	5.00, 5.95
Ala112 (F7)[e] [F14][f]	NH	9.34
	$C_\alpha H$	5.16
	$C_\beta H_3$	2.95
Ala114(F9)[e] [F16][f]	NH	9.99
	$C_\alpha H$	4.60
	$C_\beta H_3$	1.11
His117(FG3)[e] [FG2][f]	NH	7.30
	$C_\alpha H$	4.57
	$C_\beta Hs$[b]	2.08, 3.49
	$C_\delta H$	9.60 (20)[c]
	$C_\varepsilon H$	6.57
Val119(FG5)[e] [FG4][f]	NH	8.08
	$C_\alpha H$	2.60

Residue	Proton	δ_{DSS}(obs)
	$C_\beta H$	1.48
	$C_\gamma H_3$s[b]	−1.39(100),[c] −2.30(55)[c]
Tyr123(G4)[e] [G2][f]	NH	7.24
	$C_\alpha H$	3.43
	C_βHs[b]	1.55, 1.35
	C_γHs	6.56
	C_ζHs	6.50
Phe124(G5)[e] [G3][f]	NH	7.92
	$C_\alpha H$	2.94
	C_βHs[b]	3.27, 2.53
	C_δHs	6.99
	C_εHs	8.31
	$C_\zeta H$	12.20 (20)[c]
Leu127(G8)[e] [G6][f]	NH	7.65
	$C_\alpha H$	2.92
	C_βHs[b]	0.27, −0.72
	$C_\gamma H$	0.38
	$C_\delta H_3$s	−0.55, −1.30(110)[c]

[a] Chemical shifts, in ppm, referenced to DSS, in ^1H_2O, 50 mM in phosphate, pH 7.5 at 30°C.

[b] Diasterotropic protons (methyls) assigned stereospecifically on the basis of selective NOESY cross peaks, differentiated relaxation or differentiated dipolar shifts, and are listed in order (i.e., $C\beta 1H$, $C\beta 2H$, $C\gamma 1H_3$, $C\gamma 2H_3$, etc.).

[c] T_1 values, in ms, for resolved residue protons are given in parentheses.

[d] (?) indicates tentative assignment.

[e] Helical/loop positions in mammalian (i.e., axial His is F8, distal is E7, etc) Mb fold is given in parentheses.

[f] Actual helical/loop positions in Cygb are given in square brackets.

Table 3

Anisotropies and orientation of the paramagnetic susceptibility tensor of metCygb.

	C83S/C38S-metCygb[a]	WT metCygb[b]
$\Delta\chi_{ax}$	2.18±0.08[c]	2.08±0.08[c]
$\Delta\chi_{rh}$	−0.52±0.11[c]	−0.49±0.11[c]
α	80±8°	121±8°
β	6±1°	5±1°
κ	−4±10°	1±10°

[a] Coordinates for chain B in reference [11]

[b] Coordinates for metCygb in reference [12]

[c] in units × 10^{-8} m^3/mol.